

Drift Compression and Final Focus of Intense Heavy Ion Beam*

Hong Qin¹, Ronald C. Davidson¹, John J. Barnard² and Edward P. Lee³

1 Princeton Plasma Physics Laboratory, Princeton University, Princeton, New Jersey 08543

2 Lawrence Livermore National Laboratory, Livermore, California 94550

3 Lawrence Berkeley National Laboratory, Berkeley, California 94720

Abstract

The longitudinal and transverse dynamics of a heavy ion fusion beam during the drift compression and final focus phase is studied. A lattice design with four time-dependent magnets is described that focuses the entire beam pulse onto a single focal point with the same spot size.

LONGITUDINAL DRIFT COMPRESSION

In the currently envisioned configurations for heavy ion fusion, it is necessary to longitudinally compress the beam bunches by a large factor after the acceleration phase and before the beam particles are focused onto the fusion target. The objective of drift compression is to compress a long beam bunch by imposing a negative longitudinal velocity tilt over the length of the beam in the beam frame. Because the space-charge force increases as the beam is compressed, a larger focusing force is needed to confine the beam in the transverse direction. It is necessary to have a non-periodic quadrupole lattice along the beam path when the beam is undergoing longitudinal compression. In this paper, we describe the design of such a lattice with four final focusing magnets that focus the beam onto the target. The designed lattice is expected to apply for the entire beam pulse. In particular, different slices should be focused onto the same focal point at the target. This is difficult with a fixed lattice. One solution is to use a time-dependent lattice which provides a different focusing strength for different slices of the beam pulse. We demonstrate that the entire pulse can be compressed and focused onto the same focal point on the target by using four time-varying quadrupole magnets at the very beginning of drift compression. The following set of beam parameters typical of heavy ion fusion is used in the present study. We consider a Cs^+ beam with rest mass $m = 132.9$ amu, kinetic energy $(\gamma - 1)mc^2 = 2.43$ GeV, and initial beam half-length $z_{b0} = 5.85$ m. The goal is to compress the beam by a factor of 21.8. The final average current is taken to be $\langle I_f \rangle = 2254$ A.

We use a one-dimensional warm-fluid model [1, 2] to describe the longitudinal dynamics of drift compression. For the longitudinal electric field, the conventional g -factor model is adopted, with $eE_z = -(ge^2/\gamma^2) \partial\lambda/\partial z$ and $g = 2 \ln(r_w/r_b)$. Here, e is the charge, $\lambda(t, z)$ is the line density, r_w is the wall radius, and r_b is the average beam radius. We also allow for an externally applied axial focusing force $F_z = -\kappa_z z$. In the beam frame, the warm-fluid

equations for the line density $\lambda(t, z)$, longitudinal velocity $v_z(t, z)$, and longitudinal pressure $p_z(t, z)$ are given by

$$\begin{aligned} \frac{\partial\lambda}{\partial t} + \frac{\partial}{\partial z}(\lambda v_z) &= 0, \\ \frac{\partial v_z}{\partial t} + v_z \frac{\partial v_z}{\partial z} + \frac{e^2 g}{m\gamma^5} \frac{\partial\lambda}{\partial z} + \frac{\kappa_z z}{m\gamma^3} + \frac{r_b^2}{m\gamma^3 \lambda} \frac{\partial p_z}{\partial z} &= 0, \\ \frac{\partial p_z}{\partial t} + v_z \frac{\partial p_z}{\partial z} + 3p_z \frac{\partial v_z}{\partial z} &= 0. \end{aligned} \quad (1)$$

We treat g and r_b as constants for present purposes. Among all of the self-similar solutions [1] admitted by the nonlinear hyperbolic partial differential equation system (1), the parabolic self-similar solution is the most suitable for the purpose of drift compression, and has the form of [1]

$$\begin{aligned} \lambda(t, z) &= \lambda_b(t) \left(1 - \frac{z^2}{z_b^2(t)}\right), \quad v_z(t, z) = -v_{zb}(t) \frac{z}{z_b(t)}, \\ p_z(t, z) &= p_{zb}(t) \left(1 - \frac{z^2}{z_b^2(t)}\right)^2, \quad \frac{dz_b(t)}{dt} = -v_{zb}(t). \end{aligned} \quad (2)$$

Following the derivation in [1], we obtain the familiar longitudinal envelope equation

$$\frac{d^2 z_b}{ds^2} + \kappa_z z_b - K_z \frac{1}{z_b^2} - \varepsilon_l^2 \frac{1}{z_b^3} = 0, \quad (3)$$

where $s = \beta ct$ is the normalized time variable, $K_z \equiv 3N_b e^2 g / 2m\gamma^5 \beta^2 c^2$ is the effective longitudinal self-field perveance, N_b is the total number of particles in the bunch, and $\varepsilon_l \equiv (4r_b^2 W / m\gamma^3 \beta^2 c^2)^{1/2}$ is the longitudinal emittance. In the drift compression scheme considered in this paper, the longitudinal emittance is taken to be $\varepsilon_l = 1.0 \times 10^{-5}$ m, where $K_z = 2.88 \times 10^{-5}$ m, corresponding to an average final current $\langle I_f \rangle = 2254$ A, $z_{bf} = 0.268$ m, and $g = 0.81$. An initial longitudinal focusing force is imposed for $s < 150$ m so that the beam acquires a velocity tilt $z'_b = -0.0143$ at $s_b = 150$ m. The axial beam size $z_b(s)$, obtained numerically from the longitudinal envelope equation (3), is plotted together with the velocity tilt $z'_b(s)$ in Fig. 1. A pulse shaping technique has also been demonstrated so that any initial pulse shape can be shaped into a parabolic one which can then be self-similarly compressed [1, 2].

LATTICE AND TRANSVERSE DYNAMICS

For each slice in a bunched beam, the transverse dynamics in a quadrupole lattice is described approximately by

* Research supported by the U.S. Department of Energy.

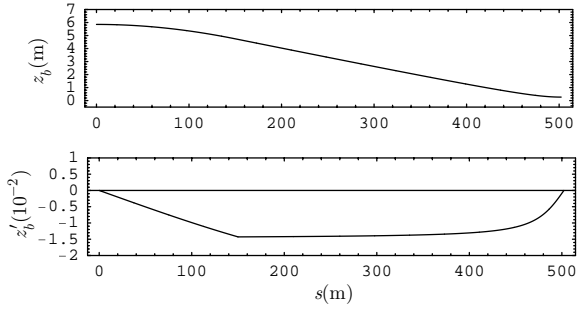


Figure 1: Dynamics of the beam half-length $z_b(s)$.

the transverse envelope equations:

$$\begin{aligned} \frac{d^2 a(s, z)}{ds^2} + \kappa_q a(s, z) - \frac{2K(s, z)}{a(s, z) + b(s, z)} - \frac{\varepsilon_x^2}{a(s, z)^3} &= 0, \\ \frac{d^2 b(s, z)}{ds^2} - \kappa_q b(s, z) - \frac{2K(s, z)}{a(s, z) + b(s, z)} - \frac{\varepsilon_y^2}{b(s, z)^3} &= 0, \end{aligned} \quad (4)$$

where $K(s, z) \equiv 2e^2 \lambda_b(s) [1 - z^2/z_b^2(s)] / m\gamma^3 \beta^2 c^2 z_b(s)$ is the transverse perveance. Here, z is the longitudinal coordinate for different slices, which enters the equations only parametrically. Because $K(s, z)$ is an increasing function of s , it is necessary to increase the strength of $\kappa_q(s)$ along the beam path to reduce the expansion of the beam radius. Since the quadrupole lattice is not periodic, the concept of a ‘‘matched beam’’ is not well defined. However, if the non-periodicity is small, we can seek an ‘‘adiabatically-matched’’ beam which, by definition, is locally matched everywhere [1].

We describe here the design of a non-periodic lattice which provides the required control of beam radius when the beam is compressed, and equally importantly, minimizes the possibility of global mismatch. The drift compression and final focus lattice should apply for all slices in a bunched beam. In particular, each slice of the beam should be focused onto the same focal point at the target. A fixed lattice designed for one slice of the beam (e.g., the central slice at $z = 0$) will not focus other slices onto the same focal point. Actually, most of the other slices cannot be focused at all due to their different perveance and emittance. Our goal can be achieved by designing a drift compression and final focus lattice for the central slice ($z = 0$), and then replacing four quadrupole magnets at the beginning of the drift compression by four time-dependent magnets whose strength varies about the design values for the central slice. The time-dependent magnets essentially provide a slightly different focusing lattice for different slices.

First, we design the drift compression and final focus lattice for the central slice at $z = 0$. It is intuitive that a lattice, which keeps both the vacuum phase advance and the depressed phase advance constant, is less likely to induce beam mismatch [3]. Constant vacuum phase advance and constant depressed phase advance requires (when $\eta \ll 1$)

$$\eta^2 \left(\frac{B'}{[B\rho]} \right)^2 L^4 = \text{const.}, \quad K \left(\frac{2L}{\langle a \rangle} \right)^2 = \text{const.}, \quad (5)$$

where η is the filling factor, L is the lattice period, B' is field gradient of the magnets, and $\langle a \rangle$ is the average beam radius. For the drift compression scheme considered here, $K_f/K_0 = 21.8$. If we allow $\langle a \rangle$ to increase by a factor of 2.33, i.e., $\langle a \rangle_f / \langle a \rangle_0 = 2.33$, we obtain $L_f/L_0 = 1/2$, and $(\eta B')_f / (\eta B')_0 = 4$. We also need to specify η , B' , and L . If we choose $L_i = L_0 \exp[-(\ln 2) s_i/s_f]$, and $B'_i = \text{const.}$, then from Eq. (5), $\eta_i = \eta_0 \exp[(\ln 4) s_i/s_f]$, where $s_i = \sum_{j=0}^{i-1} L_j$. We also choose self-consistently the following system parameters: $\sigma_v = 72^\circ$, $B'_i = 31.70 \text{ T/m}$, $L_0 = 6.72 \text{ m}$, and $\eta_0 = 0.0725$. The focusing strength of each magnet is $\hat{\kappa} = 0.38 \text{ m}^{-2}$. Let N denote the total number of quadrupole magnet sets. From $s_f = \sum_{j=0}^{N-1} L_j$, we obtain $N = 53$.

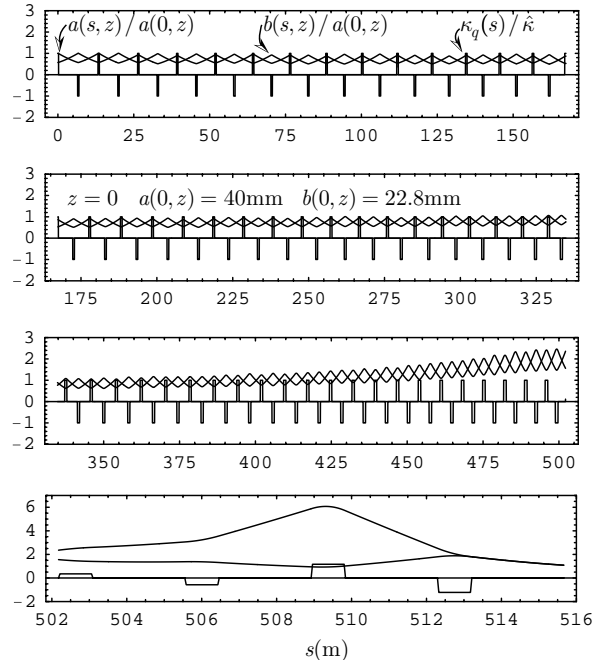


Figure 2: Envelope dynamics for the central slice.

The resulting lattice design is illustrated in Fig. 2 together with the solutions to the transverse envelope equations. After determining the non-periodic lattice layout, we search iteratively for the adiabatically-matched solutions. The solutions plotted in Fig. 2 are adiabatically-matched because the envelope is locally matched and contains no oscillations other than the local envelope oscillations. On the global scale, the beam radius increases monotonically. From the numerical solution shown in Fig. 2, the average beam size increases by a factor of 2.33, which agrees with the design assumption. The final focus magnets, consisting of four quadrupole magnets with different strength, will assure that the envelope converge in both directions at the exit of the last focusing magnet (both a' and b' are negative). Right after the last focusing magnet, the beam enters the neutralization chamber where the space-charge force is neutralized and the beam is focused onto a focal point at

$$z_{fol} = - \left. \frac{a}{\partial a / \partial s} \right|_{s=s_{ff}} = - \left. \frac{b}{\partial b / \partial s} \right|_{s=s_{ff}}, \quad (6)$$

where z_{fol} is the distance between the focal point and the exit from the last final focus magnet, and s_{ff} is the distance from the beginning of the drift compression to the exit from the last final focus magnet. It is necessary that $a/(\partial a/\partial s)$ and $b/(\partial b/\partial s)$ have the same value at $s = s_{ff}$ for a focal point to exist. The transverse spot size measured by the envelope amplitudes at the focal point a_{fol} and b_{fol} is determined by the emittance and incident angle at $s = s_{ff}$,

$$a_{fol} = \frac{\varepsilon_x}{\partial a/\partial s} \Big|_{s=s_{ff}}, \quad b_{fol} = \frac{\varepsilon_y}{\partial b/\partial s} \Big|_{s=s_{ff}}. \quad (7)$$

For the central slice at $z = 0$, we obtain $z_{fol} = 5.276$ m, and $a_{fol} = b_{fol} = 1.22$ mm.

For other slices ($z \neq 0$), the objective is to manipulate the beam and magnet configuration so that the beam particles can be focused onto a focal region with the same or smaller spot size,

$$z_{fol} = 5.276 \text{ m}, \quad a_{fol} \approx b_{fol} \lesssim 1.22 \text{ mm}. \quad (8)$$

We observe, for the line density profile $\lambda(s, z) = \lambda_b(s)[1 - z^2/z_b^2(s)]$, that the solution to the transverse envelope equations for all of the slices can be scaled down from that of the central slice according to

$$\begin{pmatrix} a(s, z) \\ b(s, z) \\ \partial a(s, z)/\partial s \\ \partial b(s, z)/\partial s \end{pmatrix} = \sqrt{1 - z^2/z_b^2(s)} \begin{pmatrix} a(s, 0) \\ b(s, 0) \\ \partial a(s, 0)/\partial s \\ \partial b(s, 0)/\partial s \end{pmatrix}, \quad (9)$$

provided the emittance is negligibly small or scales with the perveance according to $(\varepsilon_x, \varepsilon_y) \propto 1 - z^2/z_b^2(s)$. However, the emittance in general is small but not negligible, and does not scale with the perveance. In fact, during adiabatic drift compression, the emittance scales with the beam size, i.e., $\varepsilon_x \propto a$ and $\varepsilon_y \propto b$, which is assumed in the present analysis. This implies that the scaling in Eq. (9) and the requirement in Eq. (8) can't be satisfied.

One solution to this difficulty is to vary the strength of four magnets in the very beginning of the drift compression for different value of z such that the desired scaling in Eq. (9) holds at $s = s_{ff}$. Combined with Eqs. (6) and (7), this will guarantee the satisfaction of the requirement in Eq. (8). This is a viable solution because the emittance, and therefore the departure from the desired scaling, are small. Numerically, the necessary variation of the strength of the magnets is found by a 4D root-searching algorithm. Shown in Fig. 3 is the dynamics of $a(s, z)$ and $b(s, z)$ for $z/z_b(s) = 0.968$, when the strength of the 3rd, 5th, 7th and 9th magnets are modified to satisfy Eq. (9) at $s = s_{ff}$. The initial conditions are taken to be those satisfying Eq. (9) at $s = 0$. As evident for Fig. 3, a small perturbation in the strength of the magnets introduces a small envelope mismatch in such a way that Eq. (9) is satisfied at $s = s_{ff}$. We note that a similar scaling does not exist for $0 < s < s_{ff}$. Plotted in Fig. 4 are the strengths of the 3rd, 5th, 7th and 9th magnets as functions of z which are able

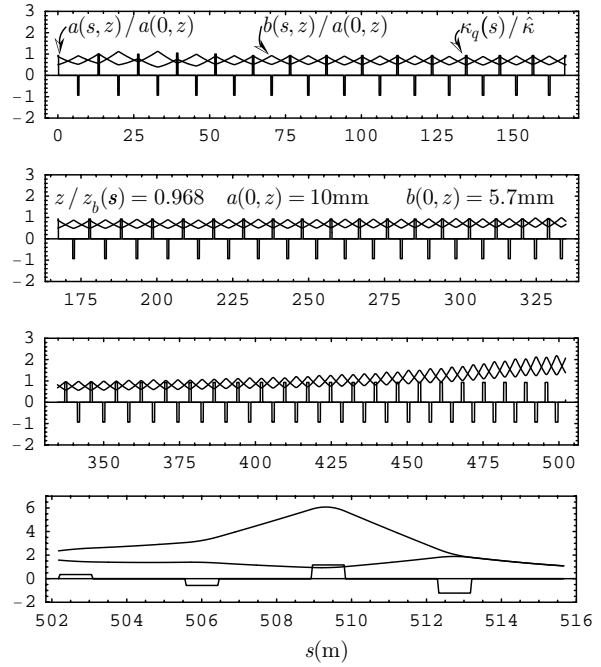


Figure 3: Envelope dynamics for the slice near the front of the beam pulse with $z/z_b(s) = 0.968$.

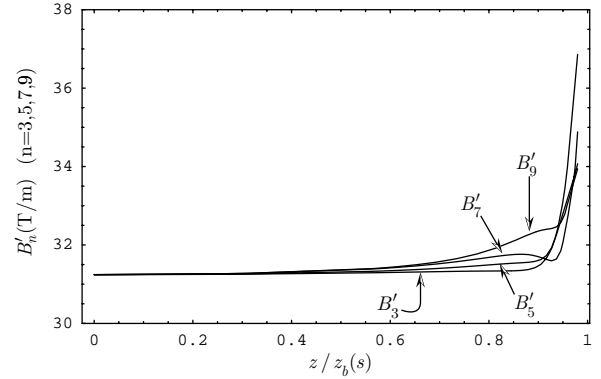


Figure 4: Strengths of the 3rd, 5th, 7th, and 9th magnets as functions of $z/z_b(s)$.

to focus the entire beam onto a focal region with the same spot size. In principle, we can use this method to correct any deviation from requirement (8) due to other possible mechanisms, such as momentum spread and magnet imperfections.

REFERENCES

- [1] H. Qin and R. C. Davidson, Phys. Rev. ST Accel. Beams **5**, 03441 (2002).
- [2] H. Qin and R. C. Davidson, Laser and Particle Beams **20**, 565 (2002).
- [3] E. P. Lee and J. J. Barnard, Laser and Particle Beams **20**, 581 (2002).